Technical Article

Group versus Phase Velocity of Shear Waves in Soft Tissues

Ultrasonic Imaging
2018, Vol. 40(6) 343–356

DOI: 10.1177/0161734618796217
journals.sagepub.com/home/uix
SAGE

Kevin J. Parker[1], Juvenal Ormachea[1], and Zaegyoo Hah[2]

Abstract

Across the varieties of waves that have been studied in physics, it is well established that group velocities can be significantly greater than or less than phase velocities measured within comparable frequency bands, depending on the particular mechanisms involved. The distinction between group and phase velocities is important in elastography, because diagnoses are made based on shear wave speed estimations from a variety of techniques. We review the general definitions of group and phase velocity and examine their specific relations within an important general class of rheological models. For the class of tissues and materials exhibiting power law dispersion, group velocity is significantly greater than phase velocity, and simple expressions are shown to interrelate the commonly measured parameters. Examples are given from phantoms and tissues.

Keywords

shear waves, elastography, ultrasound, magnetic resonance elastography, dispersion

Introduction

The classic textbooks in optics, electromagnetics, elastic waves, and acoustics have well developed discussions about the concept of phase velocity, governing the propagation of a monochromatic wave, as opposed to group velocity.[1,2] The latter pertains to the propagating shape of a wave comprising multiple frequencies. In the general textbook treatments, and in particular examples involving different kinds of waves in materials and structures, the group velocity can be lower, higher, or nearly equal to the phase velocity depending on the particular frequencies employed and mechanisms of loss, resonance, or reflections that are present. Thus, it can be difficult to generalize classical textbook results to the sub-area of shear wave propagations within soft tissues. This motivates a re-examination of fundamental relations and their most likely manifestations in soft tissues within the different elastography techniques.

In the broad field of elastography, many techniques can be classified as harmonic, transient, or quasi-static.[3] Shear wave phenomena are associated with the harmonic and transient approaches.[4] Harmonic schemes can employ sinusoidal steady-state excitations or else decompose a harmonic

[1]Department of Electrical and Computer Engineering, University of Rochester, Rochester, NY, USA
[2]Samsung Medison Co. Ltd., Seoul, Korea

Corresponding Author:
Kevin J. Parker, Department of Electrical and Computer Engineering, University of Rochester, Hopeman Building 203, Box 270126, Rochester, NY 14627-0126, USA.
Email: kevin.parker@rochester.edu

ensemble into its frequency content. Examples of single-frequency sinusoidal shear-wave excitations include some magnetic resonance elastography (MRE) approaches,[5] vibro-acoustics,[6] crawling waves,[7] and reverberant shear waves.[8,9] When these techniques estimate shear wave propagation around a single frequency, the results can be classified as phase velocity. A second class of transient and broadband shear waves results from acoustic radiation force push pulses[10] or short external push pulses.[11] When these techniques estimate the propagation of a broadband shear-wave pulse, the results can be classified as group velocity estimates.

This paper reviews the classical approaches to phase and group velocity, then applies them to some specific models, materials, and tissues that are well characterized. In particular, we demonstrate that for tissues exhibiting a power law response, the group velocity is larger than the phase velocity and that the difference depends only on the power law exponent. The predicted difference between group velocities and phase velocities is demonstrated in a tissue-mimicking phantom, and in tissues that exhibit power law behavior (liver and placenta).

Theory

General Treatment

The simplest way to view the topic is by considering one-dimensional shear-wave propagation in a linear, isotropic, homogeneous, infinite medium. In summary, using the complex exponential to represent a plane wave at frequency ω, the solution to the wave equations for a disturbance traveling in the $+x$ direction is,

$$u(x) = A\mathbf{e}^{-j(kx-\omega t)}, \tag{1}$$

where $u(x)$ is displacement, A is an amplitude, j is the imaginary unit, and k is the wavenumber. Furthermore,

$$k = \frac{\omega}{c} \tag{2}$$

and

$$c = \sqrt{\frac{G}{\rho}} \cong \sqrt{\frac{E}{3\rho}}, \tag{3}$$

where c is the wave speed, ρ is the density, G is the shear modulus, and E is the Young's modulus, the approximation $G = E/3$ valid for nearly incompressible materials. Additional details can be seen in Chapter 5 of Graff,[12] or summarized for elastography in Parker et al.[13] The important point is that in this purely elastic, lossless propagation, there is only one velocity c for all frequencies and no distinction in speeds observed between monochromatic narrowband and broadband shear-wave disturbances.

The situation changes when some loss mechanism enters the wave equation, usually through the constitutive equations of the material that is supporting the shear waves. In this case, the speed c changes with frequency (a phenomenon called "dispersion"), and the concept of group velocity is introduced, related to the slope, or derivative, of phase velocity. An excellent treatment is given in Section 1.6.1 of Graff.[2] For our purposes here, we simply note that the group velocity $v_g(\omega)$ governs the propagation of the observed wave packet of a disturbance that has multiple frequencies. Quantitatively,

$$v_g(\omega) = \frac{d\omega}{d\beta}, \tag{4}$$

where

$$\beta(\omega) = \frac{\omega}{c_p(\omega)} = \frac{2\pi}{\lambda(\omega)}, \tag{5}$$

and where c_p is the phase velocity and λ is the wavelength. Strictly speaking, this classical definition is only valid for wave packets with sufficiently limited bandwidths such that the slope $d\omega/d\beta$ is approximately constant over the bandwidth.[14] Experimentally, one can determine $\beta(\omega)$ at discrete frequencies by measuring the wavelength or the disturbance speed.[15-17] Then, a plot of β versus ω can be made and used to estimate the slope and hence the group velocity in any frequency band. This group velocity would govern the apparent speed of a multifrequency wave packet. In general, v_g can be greater than, equal to, or less than c_p depending on the specifics of the materials. Accordingly, we next examine lossy models of tissues that produce complex, frequency-dependent wavenumbers.

Lossy or viscoelastic materials like tissues can be characterized by their stress–strain relations leading to complex $E(\omega)$ and $G(\omega)$.[18] In this case, the solution to the lossy wave equation still resembles Equation (1), but now k is complex: its real component is still related to ω/c_p and its imaginary component defines an exponential decay with distance. Accordingly, we write a general form for complex, frequency-dependent shear modulus[18,19]:

$$G^*(\omega) = \left(G_d(\omega) + jG_i(\omega)\right), \tag{6}$$

where G^* is the complex modulus, G_d is the dynamic modulus, and G_i is the loss modulus. So the propagation constant

$$k = \frac{\omega}{\sqrt{\dfrac{G_d(\omega) + jG_i(\omega)}{\rho}}} = \beta - j\alpha = \frac{\omega}{c_p} - j\alpha, \tag{7}$$

and the wave now propagates as,

$$\begin{aligned} u(x) &= A\mathbf{e}^{-\alpha x}\mathbf{e}^{j(\omega t - \beta x)} \\ &= A\mathbf{e}^{-\alpha x}\mathbf{e}^{j\omega\left(t - \frac{x}{\omega/\beta}\right)}. \end{aligned} \tag{8}$$

The latter form emphasizes that this is a rightward $(+x)$ propagating wave with speed of $c_p = \omega/\beta$. Now sorting through the real and imaginary parts of Equation (7), and denoting,

$$|G| = \sqrt{G_d^2(\omega) + G_i^2(\omega)}, \tag{9}$$

we find that

$$\beta = \left[\omega\sqrt{\frac{\rho}{|G|}}\right]\left[\frac{1}{2}\left(1 + \frac{G_d(\omega)}{|G|}\right)\right]^{1/2}. \tag{10}$$

The phase velocity is a function of frequency,

$$c_p = \left[\sqrt{\frac{|G|}{\rho}}\right]\left[\frac{1}{2}\left(1 + \frac{G_d(\omega)}{|G|}\right)\right]^{-1/2}, \tag{11}$$

and the attenuation coefficient has a leading term directly proportional to the first power of frequency:

$$\alpha = \left[\omega\sqrt{\frac{\rho}{|G|}}\right]\left[\frac{1}{2}\left(1-\frac{G_d(\omega)}{|G|}\right)\right]^{1/2}. \tag{12}$$

Particular forms of these for some tissue models can be found in Carstensen and Parker.[20] In more general terms, the constraints of causality impose specific inter-relationships between attenuation and phase velocity as a function of frequency. These can be captured in the form of Kramers–Kronig relations,[21,22] and through Hilbert transform relations.[23]

Specific Relations under a Power Law Rheological Model

It should be noted that a power law behavior governing the complex modulus has been observed in different materials,[18] and can be modeled by a number of theoretical approaches.[24-26] A key element is the concept of multiple mechanisms operating across a range of scales or time constants.[27,28] Multiscale ladders or mechanisms can be modeled by the fractional derivative operators,[29] and a power law results from the two-parameter microchannel flow model, equivalent to the generalized Maxwell model or the Kelvin–Voigt fractional derivative (KVFD) model with small E_0.[26] Other models have been derived from the application of fractional derivative operators[30] in the wave equation. Alternatively, the power law behavior of viscoelastic tissues may be linked to the architecture of tissue, particularly cross-linked or entangled structures.[31,32]

The frequency-domain response of a general power law model can be written as a stress (σ) – strain (ε) relationship[18]:

$$\sigma(\omega) = E_0 (j\omega)^a \varepsilon(\omega), \tag{13}$$

where ω is radial frequency and is taken to be positive, that is, $\omega \geq 0$. The complex modulus as a function of frequency $E(\omega)$ is then obtained by

$$E(\omega) = \frac{\sigma(\omega)}{\varepsilon(\omega)} = \left[E_0 \cos\left(\frac{\pi a}{2}\right)\omega^a\right] + j\left[E_0 \sin\left(\frac{\pi a}{2}\right)\omega^a\right]. \tag{14}$$

The magnitude of $E(\omega)$ can be expressed as

$$|E(\omega)| = E_0\omega^a. \tag{15}$$

It should be noted here that Equations (13) to (15) are approximations to small strain behavior, observed over a limited window of the frequency domain. Limits of behavior near zero frequency and infinity must be treated separately.[18] From Equation (14), we get the storage modulus, $E'(\omega)$, which is the real part of the complex modulus, and the loss modulus $E''(\omega)$, which is the imaginary part:

$$E'(\omega) = E_0 \cos\left(\frac{\pi a}{2}\right)\omega^a, \tag{16}$$

$$E''(\omega) = E_0 \sin\left(\frac{\pi a}{2}\right)\omega^a. \tag{17}$$

The storage modulus is related to the elasticity of soft tissue, whereas the loss modulus is related to viscoelasticity.

$G(\omega)$ will be approximately $E(\omega)/3$ for incompressible solids and $G_0 = E_0/3$, and so $G_d(\omega)$ and $G_i(\omega)$ have the same form as Equations (16) and (17), respectively. Substituting these into Equations (11) and (12), we have,

$$c_p = \left(\omega^{\frac{a}{2}}\right)\left(\sqrt{\frac{G_0}{\rho}}\right)\left[\frac{1}{2}\left(1+\cos\left(\frac{\pi a}{2}\right)\right)\right]^{-1/2} \tag{18}$$

and

$$\alpha = \left(\omega^{\left(1-\frac{a}{2}\right)}\right)\left(\sqrt{\frac{\rho}{G_0}}\right)\left[\frac{1}{2}\left(1-\cos\left(\frac{\pi a}{2}\right)\right)\right]^{1/2}. \tag{19}$$

This form is also consistent with the high frequency approximation of a fractional wave equation.[33] In more practical terms, we rewrite this as,

$$c_p = \omega^{\frac{a}{2}} c_1 \tag{20}$$

and

$$\alpha = \frac{\omega^{\left(1-\frac{a}{2}\right)}}{c_1}\left(\frac{\pi a}{8}\right), \tag{21}$$

where c_1 is the phase velocity measured at $\omega = 1$ rad/s, and a small value of a is assumed in reducing the cosine terms to Equation (21). In practice, the approximation is accurate to within 5% for $a < 0.3$.

Note that Equations (20) and (21) comprise two equations in four unknowns: c_p, a, α, and c_1. Thus, estimates of any two can be used to calculate the other two, producing a complete characterization of the material under the power law model that is also consistent with the Kramers–Kronig law.[22]

We now apply the general rule of group velocity to the particular power law viscoelastic behavior.

$$v_g = \frac{d\omega}{d\beta}. \tag{22}$$

Let

$$c_p(\omega) = c_1\omega^{\frac{a}{2}}, \tag{23}$$

$$\beta = \frac{\omega}{c_p(\omega)} = \frac{1}{c_1}\omega^{\left(1-\frac{a}{2}\right)}, \tag{24}$$

and

$$\frac{d\beta}{d\omega} = \frac{1-\frac{a}{2}}{c_1\omega^{\frac{a}{2}}}. \tag{25}$$

Thus,

$$v_g = \left[\frac{1}{1-\frac{a}{2}}\right] c_p(\omega), \tag{26}$$

and so *group velocity* v_g *is significantly higher than phase velocity* c_p, by a factor in the typical range of 1.1 to 1.2 or higher in many soft tissues where $0 < a < 0.3$.[15,34,35]

In many cases, measurements are obtained over a limited bandwidth, and the simplest measurement of dispersion is the slope $\Delta c_p / \Delta\omega$. For power law media, we see from Equation (23) that

$$\frac{dc_p(\omega)}{d\omega} = \frac{\frac{a}{2} c_1}{\omega^{\left(1-\frac{a}{2}\right)}}, \tag{27}$$

and this slope varies strongly, higher at low frequencies. This has been observed in human livers (see Table 2 of Parker et al.[35]). Within the framework of the power law media, a simplification results if one plots the c_p versus ω data on a log–log scale. In this case, the slope will be independent of frequency,

$$\frac{d(\log c_p)}{d(\log \omega)} = \frac{a}{2}. \tag{28}$$

In other words, the slope or dispersion as measured from a log–log plot of $c_p(\omega)$ versus ω will be constant across different frequency bands, whereas the slope from a linear plot will vary with frequency.

Method

A collection of techniques has been used in our laboratories to obtain group velocity or phase velocity estimates of shear waves. These will be described individually in the following paragraphs.

Crawling Wave Sonoelastography (CWS)

In CWS, two opposing shear-wave vibration sources are operated at slightly offset frequencies and produce a slowly moving interference pattern, termed *crawling wave*. The apparent velocity of the crawling waves is proportional to the underlying shear phase velocity of the media. CWS was applied in an ex vivo beef liver sample at low vibration frequencies (40-280 Hz). Further details of this technique can be found in Ormachea et al.[36]

Single Tracking Location–Shear Wave Elastography (STL-SWE)

STL-SWE is a modality based on acoustic radiation force. In STL-SWE, the acoustic radiation push is applied at two locations, typically 2 to 4 mm apart, and the induced shear waves are tracked at one location. The velocity data, associated with the two pushes, is cross-correlated to extract the arrival time difference between both waves to obtain the group velocity. Separately, the phase velocity was obtained by taking the difference of phase of the Fourier transforms of the shear wave created by the two acoustic radiation force pushes. STL-SWE was applied in an ex vivo beef liver sample and perfused placenta tissues using a 4.5 MHz center frequency linear array. A vasoactive substance was also employed in the placenta experiments. After baseline

perfusion, U46619 (Caymen Chemical Co., Ann Arbor, Michigan, USA), a thromboxane agonist and a potent vasoconstrictor, was injected into the fetal artery at a standard dose (1 mL, 10^{-6} M) as a bolus. Thus, STL-SWE measurements were obtained in the same region of interest before and after vasoconstriction. Further details of these experiments can be found in Ormachea et al.[36] and McAleavey et al.[37] for the ex vivo beef liver and the perfused placenta tissue, respectively.

Reverberant–Shear Wave Elastography (R-SWE)

Recently, a new method was proposed for tissue stiffness estimation by creating a reverberant shear wave field propagating in all directions within the media.[8,9] These reverberant conditions lead to simple solutions, facile implementation, and rapid phase velocity estimation of tissue. A Verasonics ultrasound system (V-1, Verasonics Inc., Kirkland, Washington, USA) connected to a linear array ultrasound transducer (Model L7-4, ATL Inc., Bothell, Washington, USA) were used to track the induced displacements. The center frequency was 5 MHz, 10 cycles of displacements were acquired, and the tracking pulse repetition frequency (PRF) was set to acquire at least 18 samples per cycle. Vibration frequency ranges of 80 to 220 Hz, and 100 to 240 Hz were applied to a Computerized Imaging Reference Systems (CIRS) viscoelastic phantom and an in vivo normal human liver, respectively. In cases where R-SWE is compared with other methods from the Siemens or Samsung scanners, a standard right intercostal oblique view of the right lobe of the liver was used to ensure a similar region of interest. The in vivo human liver scans were conducted under the requirements of informed consent and the University of Rochester Institutional Review Board.

Samsung Group Velocity (SGV) Estimates

A Samsung ultrasound system (model RS85, Samsung Medison, Seoul, South Korea) and a curved array ultrasound transducer (model CAI-7A, Samsung Medison, Seoul, South Korea) were used to produce push beams and track the induced displacements. In this experiment, fewer than 100 central elements of the transducer were used to transmit focused push beams (center frequency = 2.5 MHz, 130 μs push duration, multi-focal depth along an axial line extending over 30 mm of increasing depth). After push transmission, the Samsung system immediately switched to plane wave imaging mode (center frequency = 2.5 MHz). Some averaging over depth and noise-reduction filtering are applied to the displacement and wave speed estimates; the fine details are proprietary to Samsung. The Samsung system was used to obtain 10 individual shear wave group velocity estimates in a CIRS viscoelastic phantom and an in vivo normal human liver under the requirements of informed consent and the University of Rochester Institutional Review Board.

To summarize the approaches and acronyms, we can obtain group velocity estimates from STL-SWE and SGV methods following push pulses. Alternatively, we can obtain phase velocity estimates from CWS and R-SWE using external continuous sources, or from the Fourier decomposition STL-SWE waveforms. Finally, a standard rheological test, the stress-relaxation measurement, can be utilized as an independent assessment as follows.

Mechanical Measurements (MM)

Stress relaxation measurements were performed in the ex vivo beef liver. Cylindrical samples (approximately 30 mm in diameter × 38 mm in length) were acquired using a custom-made coring knife from the liver lobe that was utilized on the same day for the other measurements. Eight cylindrical samples were carefully selected to avoid large-scale vessels or ligaments. The samples were stored in normal (0.9%) saline for less than two hours until mechanical tests were

performed. Similar to Zhang et al.[34] and Ormachea et al.,[36] the stress relaxation curve of each sample was fitted to the KVFD model using standard nonlinear least squares procedures. Further details of this experiment can be found in Ormachea et al.[36]

Results

Experimental results demonstrate that the group velocity obtained from single tracking location with cross-correlation of shear wave packets, and group velocity obtained from the Samsung proprietary tracking of shear wave packets, are consistently above phase velocity measurements of the same material. Figure 1 provides the results for the CIRS viscoelastic phantom and an in vivo liver from a normal subject obtained from a Samsung scanner. The SGV group velocity mean and standard deviation are assigned to the peak frequency of the broadband shear wave pulse (shown as a vertical blue line). The horizontal blue line represents the −6-dB spectral magnitude of the shear-wave pulse. Phase velocities estimated within the same materials are shown as a dispersion curve comprising measurements at discrete frequencies between 80 and 240 Hz using the R-SWE approach and a corresponding power law fit to Equation (23). The gray band is the prediction of group velocity using Equation (26) applied to the power law fit of R-SWE phase velocities. The CIRS phantom, which has a proprietary composition, demonstrates that the group velocity is 1.62 higher than the power law curve fit obtained from R-SWE data, whereas the liver is 1.36 higher, roughly corresponding to a power law fit of $a/2 = 0.48$ and $a/2 = 0.47$, respectively. According to Equation (26), these power laws would predict a higher increase of 1.89.

A more extensive study of multiple methods in fresh beef liver is shown in Figure 2. In this case, the group velocity is approximately 1.13 times higher than the power law curve fit obtained from the averaged phase velocity at 120 Hz, corresponding to the KVFD power law fit of $a/2 = 0.12$.

The results from perfused, living, placenta postdelivery are shown in Figure 3. In this case, a baseline perfusion has a lower power law curve fit of $a/2 = 0.15$, and a modest elevation of STL-SWE group velocity. In comparison, after a potent vasoconstrictor was administered, the power law fit of dispersion raised to $a/2 = 0.31$. The group velocity is 1.13 and 1.34 times higher than the power law curve fits obtained from STL-SWE data, for the baseline and vasoconstrictor cases, respectively. This compares with predictions from Equation (26) of 1.17 and 1.45 times the phase velocity, respectively.

Thus, in the CIRS viscoelastic phantom, in ex vivo beef liver, and in living normal liver and placenta, the group velocity is seen to be higher than the phase velocity and within a range predicted by Equation (26) under the assumption that a simple power law behavior governs the linear rheological response of the tissue under shear-wave propagation.

Discussion

There are now a large variety of approaches to imaging the elastic properties of tissues,[3,13] operating with different frequency ranges and different processing steps for estimating either group velocity or else phase velocity. Within this broad scope, it is a challenge to reconcile the different measurements obtained. For example, a review of brain tissue measurements from MRE reported shear stiffness estimates in the 10 to 60 Hz range from various groups ranging from 0.6 kPa to nearly 3.0 kPa.[38] In cases where a power law model has been explicitly applied to the brain, estimates of the power law parameter are also wide-ranging, from $0.2 < a < 1.2$.[32,39,40] Even in liver, a wide range of normal liver stiffness values is considered "normal," from under 2 to nearly 3 kPa in MRE studies.[41] The wide range of measurements includes biological variability and experimental errors and conditions. The precise frequency band and choice of group versus phase velocity estimators will clearly shift estimates up or down.

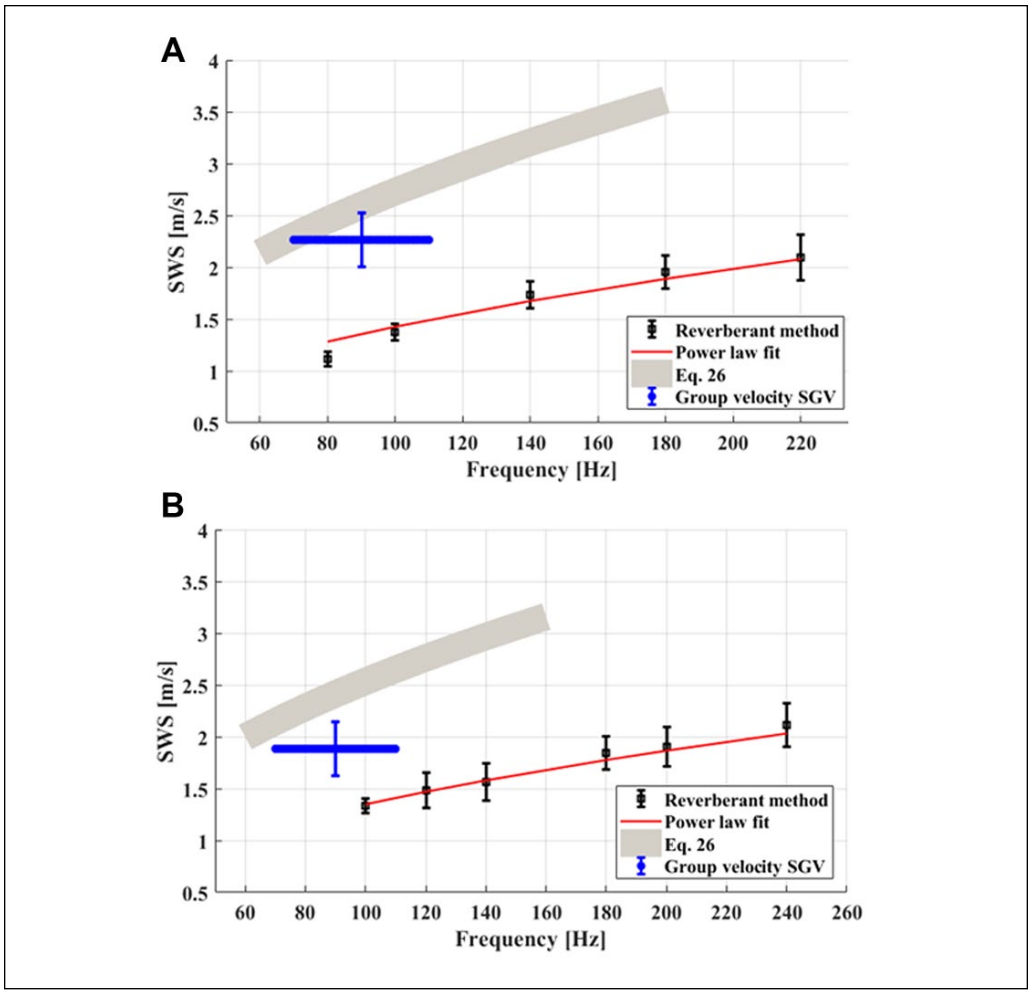

Figure 1. Shear-wave speed versus frequency measured in (a) the CIRS viscoelastic phantom, and (b) the normal human liver using shear-wave tracking (SGV) estimates and R-SWE at discrete frequencies. The corresponding group velocity estimates obtained from tracking the shear-wave pulse are assigned to the peak frequency of their Fourier-transformed signals. The shear wave pulse −6-dB spectral bandwidth is shown in the blue horizontal strip surrounding the group velocity. Red curved lines correspond to a power law fitting of phase velocity showing $c_1 = 0.07$ and $a/2 = 0.48$ for the CIRS phantom and $c_1 = 0.07$ and $a/2 = 0.47$ for the human liver. Phase velocity data points show the mean (box) and standard deviation (upper and lower bars) from 10 measurements. Gray shadow curves represent group velocity estimates predicted using Equation (26) as applied to the power law fit of the phase velocity data.

However, within the framework of a viscoelastic material exhibiting power law behavior over a meaningful frequency range (say 1 to 500 Hz shear-wave frequencies), the interrelationships simplify. In these kinds of soft tissues, the group velocity will be higher than the phase velocity by a factor of $1/\left(1-a/2\right)$, roughly a factor of 1.1 to 1.2 or higher for many healthy soft tissue specimens.[34,42] Furthermore, attenuation and dispersion will be related simply by power laws involving a, and assuming accurate measurements of parameters at one frequency are obtained, extrapolations to other frequency ranges are also accomplished simply by power law relations.

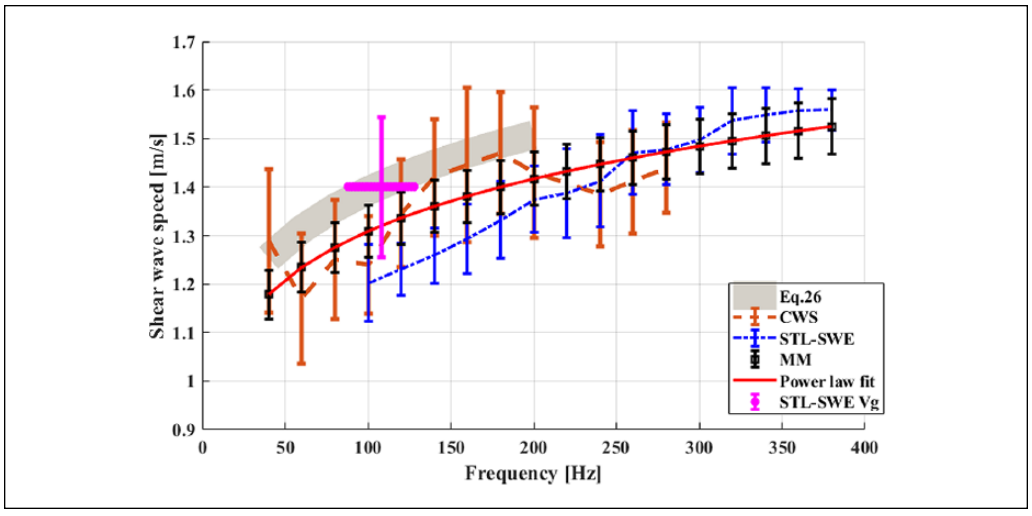

Figure 2. Comparison plots of CWS, STL-SWE, and stress-relaxation measurements (MM) using the KVFD model for an ex vivo beef liver experiment. The corresponding STL-SWE group velocity frequency was set to the peak frequency of its Fourier-transformed signals with its horizontal bar indicating the −6-dB bandwidth of the shear-wave pulse. The red curved line corresponds to a power law fit showing $c_1 = 0.63$ and $a/2 = 0.12$ for the MM results. Phase velocity data points show the mean (box) and standard deviation (upper and lower bars) from 10 measurements. The gray shadow curves represent group velocity estimates predicted using Equation (26) as applied to the phase velocity data.

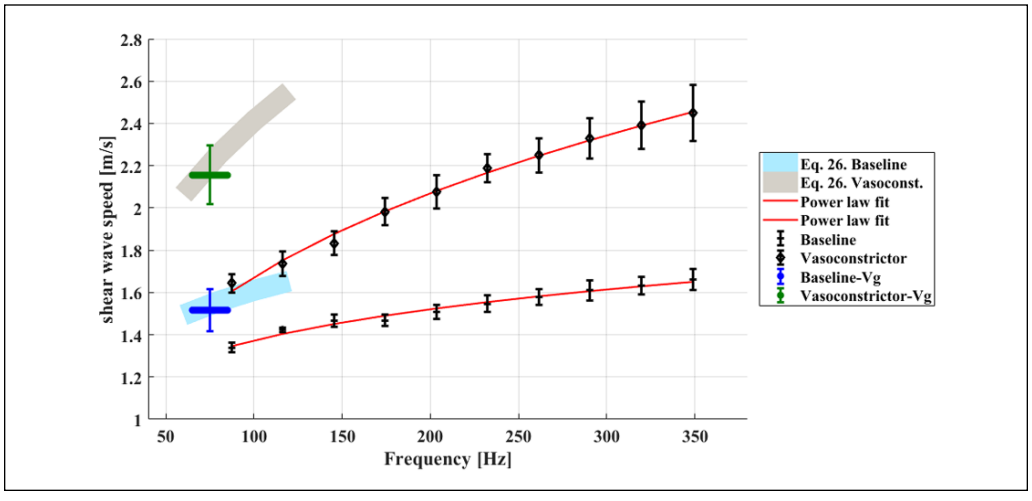

Figure 3. Shear-wave speed versus frequency for one in vitro perfused placenta using STL-SWE elastography. Administration of a potent vasoconstrictor agent results in a corresponding increase in shear-wave speed (upper curve). The black dots correspond to phase velocity and the blue and green symbols to group velocity results. Their horizontal extent indicates the −6-dB bandwidth of the shear wave pulse. Phase velocity data points show the mean (box) and standard deviation (upper and lower bars) from 10 measurements. Red curve lines correspond to a power law fitting showing $c_1 = 0.53$ and $a/2 = 0.15$ for the baseline experiments, and $c_1 = 0.23$ and $a/2 = 0.31$ for the vasoconstrictor experiments. The gray and light blue shadow curves represent group velocity estimates predicted using Equation (26) and the power law fits, applied to the baseline and vasoconstrictor cases, respectively.

Some limitations of this study can be noted. The classical concept of group velocity expressed as Equation (4) will apply closely to wave packets with bandwidths that are sufficiently limited such that the dispersion slope can be approximated by a constant. However, as Equations (22) to (28) imply, for a power law material, the dispersion slope is a gradually increasing function of frequency and power law parameter a. Thus, for shear-wave packets with large percentage bandwidths, the interpretation of group-velocity estimators becomes more complicated. In these cases, the more sophisticated method of stationary phase has been applied[12,43] and may be useful for refining comparisons.

Although we have numerous examples of soft normal tissues exhibiting power law viscoelastic behavior, we do not currently know which pathological changes would require other models. For example, power law viscoelastic behavior is consistent with the KVFD model where the discrete parallel element E_0 is set to zero; however, in the case of high-grade liver fibrosis, an interconnecting fibrotic mesh could exhibit a behavior that would require a nonzero E_0. If that were the case, the specific group velocity relation of Equation (26) would no longer hold, and one would have to recalculate the group velocity from the updated viscoelastic model. Furthermore, tissues that exhibit anisotropic and nonlinear behavior are not captured by the simple models considered in this paper, and would require further investigation.

Another limitation of these results is that the propagation equations pertain to waves in an organ that is large compared with the shear wavelengths, and not subject to strong interactions from geometric effects as is the case with plates and rods. In these cases, the dispersion curves are affected by the dimensions and shapes of the small structures and can be quite complicated functions of frequency. For an overview, see Chapter 8 of Graff.[44] In special structures such as the cornea of the eye and the arterial walls, Rayleigh waves and other bounded structural wave propagation modes have been described[45-50]; these special cases require specific case analysis of group velocity. For example, Wear[51] found that in human calcaneus bone, phase velocity decreased with frequency, and phase velocity was greater than group velocity: the opposite of results for soft tissues reported herein.

We also note that the power law models may be observed over many decades of frequency but with restrictions and mathematical issues related to causality,[19,24,52,53] and behavior as frequency approaches zero[33] or at higher frequencies where additional mechanisms become significant.[54] These topics involve deeper issues and theorems and are beyond the scope of this paper.

Within the framework of power law viscoelasticity, the interrelationship between frequency, attenuation, wavenumber, phase velocity, and group velocity all simplify to short expressions involving the power law parameter a. Given estimates of any two, the others can be specified. This enables a lawful conversion of one set of measurements to another set including different frequency bands.

Conclusion

In the presence of dispersion, group velocity is not the same as phase velocity, and many examples are available from physics and optics where group velocity is greater than, equal to, or less than phase velocity in some range depending on the material and properties in question. We demonstrate that for the wide class of soft tissues that exhibit power law viscoelastic behavior, group velocity is greater than phase velocity, typically by a factor of 10% to 20% or higher in tissues such as the liver. This is good news and bad news. The bad news is that results from laboratories and clinical studies that measure group velocity will never match the results from others measuring phase velocity in the same shear-wave frequency band. However, standardization efforts and comparisons across imaging platforms can converge for closely related techniques.[55,56] The good news is that conversions between techniques and from one frequency band to another

are possible and are simple so long as the tissues or materials in question are reasonably approximated by power law viscoelasticity.

Acknowledgments

We are grateful for support from Samsung Medison Co. Ltd. and for the loan of equipment. The authors also thank Professor Stephen McAleavey and Dr. Jonathan Langdon for their expertise and advice on single-tracking location measurements.

Declaration of Conflicting Interests

The author(s) declared no potential conflicts of interest with respect to the research, authorship, and/or publication of this article.

Funding

The author(s) received no financial support for the research, authorship, and/or publication of this article.

ORCID iD

Kevin J. Parker https://orcid.org/0000-0002-6313-6605

References

1. Brillouin L. Wave Propagation and Group Velocity. New York: Academic Press; 1960. xi.
2. Graff KF. Wave Motion in Elastic Solids, chap. 1. Oxford, UK: Clarendon Press; 1975.
3. Doyley MM. Model-based elastography: a survey of approaches to the inverse elasticity problem. Phys Med Biol. 2012;57(3):R35-R73.
4. Parker KJ, Taylor LS, Gracewski S, Rubens DJ. A unified view of imaging the elastic properties of tissue. J Acoust Soc Am. 2005;117(5):2705-12.
5. Muthupillai R, Lomas DJ, Rossman PJ, Greenleaf JF, Manduca A, Ehman RL. Magnetic-resonance elastography by direct visualization of propagating acoustic strain waves. Science. 1995;269(5232):1854-7.
6. Fatemi M, Greenleaf JF. Ultrasound-stimulated vibro-acoustic spectrography. Science. 1998;280 (5360):82-5.
7. Wu Z, Hoyt K, Rubens DJ, Parker KJ. Sonoelastographic imaging of interference patterns for estimation of shear velocity distribution in biomaterials. J Acoust Soc Am. 2006;120(1):535-45.
8. Parker KJ, Ormachea J, Zvietcovich F, Castaneda B. Reverberant shear wave fields and estimation of tissue properties. Phys Med Biol. 2017;62(3):1046-61.
9. Ormachea J, Castaneda B, Parker KJ. Shear wave speed estimation using reverberant shear wave fields: implementation and feasibility studies. Ultrasound Med Biol. 2018;44(5):963-77. doi:10.1016/j.ultrasmedbio.2018.01.011.
10. Sarvazyan AP, Rudenko OV, Swanson SD, Fowlkes JB, Emelianov SY. Shear wave elasticity imaging: a new ultrasonic technology of medical diagnostics. Ultrasound Med Biol. 1998;24(9):1419-35.
11. Catheline S, Thomas JL, Wu F, Fink MA. Diffraction field of a low frequency vibrator in soft tissues using transient elastography. IEEE Trans Ultrason Ferroelectr Freq Control. 1999;46(4):1013-9.
12. Graff KF. Wave Motion in Elastic Solids, chap. 5. Oxford, UK: Clarendon Press; 1975.
13. Parker KJ, Doyley MM, Rubens DJ. Imaging the elastic properties of tissue: the 20 year perspective. Phys Med Biol. 2011;56(1):R1-R29.
14. Fitzpatrick R. Oscillations and Waves: An Introduction, chap. 9. Boca Raton, FL: Taylor & Francis; 2013.
15. Barry CT, Hah Z, Partin A, Mooney RA, Chuang KH, Augustine A, et al. Mouse liver dispersion for the diagnosis of early-stage Fatty liver disease: a 70-sample study. Ultrasound Med Biol. 2014;40(4):704-13.
16. Meemon P, Yao J, Chu YJ, Zvietcovich F, Parker KJ, Rolland JP. Crawling wave optical coherence elastography. Opt Lett. 2016;41(5):847-50.

17. Zvietcovich F, Rolland JP, Yao J, Meemon P, Parker KJ. Comparative study of shear wave-based elastography techniques in optical coherence tomography. J Biomed Opt. 2017;22(3):35010.
18. Lakes RS. Viscoelastic Solids, chap. 2. Boca Raton, FL: CRC Press; 1999.
19. Zhang W, Holm S. Estimation of shear modulus in media with power law characteristics. Ultrasonics. 2016;64:170-6.
20. Carstensen EL, Parker KJ. Physical models of tissue in shear fields. Ultrasound Med Biol. 2014;40(4):655-74.
21. Cobbold RSC. Foundations of Biomedical Ultrasound, sec. 3.10.1. New York: Oxford University Press; 2007. xix.
22. Szabo TL. Causal theories and data for acoustic attenuation obeying a frequency power-law. J Acoust Soc Am. 1995;97(1):14-24.
23. Bracewell RN. The Fourier Transform and Its Applications, chap. 12. McGraw-Hill Series in Electrical Engineering Circuits and Systems. 1st ed. New York: McGraw-Hill; 1965, p. 112.
24. Szabo TL, Wu J. A model for longitudinal and shear wave propagation in viscoelastic media. J Acoust Soc Am. 2000;107(5, pt. 1):2437-46.
25. Chen W, Holm S. Modified Szabo's wave equation models for lossy media obeying frequency power law. J Acoust Soc Am. 2003;114(5):2570-4.
26. Parker KJ. A microchannel flow model for soft tissue elasticity. Phys Med Biol. 2014;59(15):4443-57.
27. Fung YC. Biomechanics: Mechanical Properties of Living Tissues, chap. 7. New York: Springer-Verlag; 1981. xii.
28. Liu Z, Bilston L. On the viscoelastic character of liver tissue: experiments and modelling of the linear behaviour. Biorheology. 2000;37(3):191-201.
29. Sokolov IM, Klafter J, Blumen A. Fractional kinetics. Phys Today. 2002;55(11):48-54.
30. Holm S, Nasholm SP. Comparison of fractional wave equations for power law attenuation in ultrasound and elastography. Ultrasound Med Biol. 2014;40(4):695-703.
31. Guo J, Posnansky O, Hirsch S, Scheel M, Taupitz M, Braun J, et al. Fractal network dimension and viscoelastic powerlaw behavior: II. An experimental study of structure-mimicking phantoms by magnetic resonance elastography. Phys Med Biol. 2012;57(12):4041-53.
32. Sack I, Johrens K, Wurfel J, Braun J. Structure-sensitive elastography: on the viscoelastic powerlaw behavior of in vivo human tissue in health and disease. Soft Matter. 2013;9(24):5672-80.
33. Holm S, Sinkus R. A unifying fractional wave equation for compressional and shear waves. J Acoust Soc Am. 2010;127(1):542-8.
34. Zhang M, Castaneda B, Wu Z, Nigwekar P, Joseph JV, Rubens DJ, et al. Congruence of imaging estimators and mechanical measurements of viscoelastic properties of soft tissues. Ultrasound Med Biol. 2007;33(10):1617-31.
35. Parker KJ, Partin A, Rubens DJ. What do we know about shear wave dispersion in normal and steatotic livers? Ultrasound Med Biol. 2015;41(5):1481-7.
36. Ormachea J, Lavarello RJ, McAleavey SA, Parker KJ, Castaneda B. Shear wave speed measurements using crawling wave sonoelastography and single tracking location shear wave elasticity imaging for tissue characterization. IEEE Trans Ultrason Ferroelectr Freq Control. 2016;63(9):1351-60.
37. McAleavey SA, Parker KJ, Ormachea J, Wood RW, Stodgell CJ, Katzman PJ, et al. Shear wave elastography in the living, perfused, post-delivery placenta. Ultrasound Med Biol. 2016;42(6):1282-8.
38. Hiscox LV, Johnson CL, Barnhill E, McGarry MD, Huston J, van Beek EJ, et al. Magnetic resonance elastography (MRE) of the human brain: technique, findings and clinical applications. Phys Med Biol. 2016;61(24):R401-R37.
39. Streitberger KJ, Wiener E, Hoffmann J, Freimann FB, Klatt D, Braun J, et al. In vivo viscoelastic properties of the brain in normal pressure hydrocephalus. NMR Biomed. 2011;24(4):385-92.
40. Testu J, McGarry MDJ, Dittmann F, Weaver JB, Paulsen KD, Sack I, et al. Viscoelastic power law parameters of in vivo human brain estimated by MR elastography. J Mech Behav Biomed Mater. 2017;74:333-41.
41. Srinivasa Babu A, Wells ML, Teytelboym OM, Mackey JE, Miller FH, Yeh BM, et al. Elastography in chronic liver disease: modalities, techniques, limitations, and future directions. Radiographics. 2016;36(7):1987-2006.

42. Parker KJ, Ormachea J, McAleavey SA, Wood RW, Carroll-Nellenback JJ, Miller RK. Shear wave dispersion behaviors of soft, vascularized tissues from the microchannel flow model. Phys Med Biol. 2016;61(13):4890-903.
43. Papoulis A. The Fourier Integral and Its Applications, chap. 7. New York: McGraw-Hill; 1987.
44. Graff KF. Wave Motion in Elastic Solids, chap. 8. Oxford: Clarendon Press; 1975.
45. Zvietcovich F, Yao J, Rolland JP, Parker KJ (eds.). Experimental classification of surface waves in optical coherence elastography. In: SPIE BiOS. SPIE; 2016. https://www.spiedigitallibrary.org/conference-proceedings-of-spie/9710/97100Z/Experimental-classification-of-surface-waves-in-optical-coherence-elastography/10.1117/12.2211420.full?SSO=1
46. Li C, Guan G, Reif R, Huang Z, Wang RK. Determining elastic properties of skin by measuring surface waves from an impulse mechanical stimulus using phase-sensitive optical coherence tomography. J R Soc Interface. 2012;9(70):831-41.
47. Nenadic IZ, Urban MW, Bernal M, Greenleaf JF. Phase velocities and attenuations of shear, Lamb, and Rayleigh waves in plate-like tissues submerged in a fluid (L). J Acoust Soc Am. 2011;130(6):3549-52.
48. Mercado KP, Langdon J, Helguera M, McAleavey SA, Hocking DC, Dalecki D. Scholte wave generation during single tracking location shear wave elasticity imaging of engineered tissues. J Acoust Soc Am. 2015;138(2):EL138-44.
49. Li C, Guan G, Huang Z, Wang RK, Nabi G (eds.). Full skin quantitative optical coherence elastography achieved by combining vibration and surface acoustic wave methods. In: SPIE BiOS. SPIE; 2015. https://www.spiedigitallibrary.org/conference-proceedings-of-spie/9322/93220O/Full-skin-quantitative-optical-coherence-elastography-achieved-by-combining-vibration/10.1117/12.2075666.full
50. Zhang X, Osborn TG, Pittelkow MR, Qiang B, Kinnick RR, Greenleaf JF. Quantitative assessment of scleroderma by surface wave technique. Med Eng Phys. 2011;33(1):31-7.
51. Wear KA. Group velocity, phase velocity, and dispersion in human calcaneus in vivo. J Acoust Soc Am. 2007;121(4):2431-7.
52. Kelly JF, McGough RJ, Meerschaert MM. Analytical time-domain Green's functions for power-law media. J Acoust Soc Am. 2008;124(5):2861-72.
53. Parker KJ. Real and causal hysteresis elements. J Acoust Soc Am. 2014;135(6):3381-9.
54. Parker KJ. The microchannel flow model under shear stress and higher frequencies. Phys Med Biol. 2017;62(8):N161-7.
55. Palmeri M, Nightingale K, Fielding S, Rouze N, YuFeng D, Lynch T, et al (eds.). RSNA QIBA ultrasound shear wave speed Phase II phantom study in viscoelastic media. In: Ultrasonics Symposium (IUS), 2015 IEEE International, Taipei, Taiwan, 21-24 October 2015, pp.1-4. https://ieeexplore.ieee.org/document/7329478/
56. Shin HJ, Kim MJ, Kim HY, Roh YH, Lee MJ. Comparison of shear wave velocities on ultrasound elastography between different machines, transducers, and acquisition depths: a phantom study. Eur Radiol. 2016;26(10):3361-7.